NASA/TM—2019-220184

Vortex Radiometry: Fundamental Concepts

Peter J. Schemmel
Glenn Research Center, Cleveland, Ohio

April 2019

NASA STI Program . . . in Profile

Since its founding, NASA has been dedicated to the advancement of aeronautics and space science. The NASA Scientific and Technical Information (STI) Program plays a key part in helping NASA maintain this important role.

The NASA STI Program operates under the auspices of the Agency Chief Information Officer. It collects, organizes, provides for archiving, and disseminates NASA's STI. The NASA STI Program provides access to the NASA Technical Report Server—Registered (NTRS Reg) and NASA Technical Report Server—Public (NTRS) thus providing one of the largest collections of aeronautical and space science STI in the world. Results are published in both non-NASA channels and by NASA in the NASA STI Report Series, which includes the following report types:

- TECHNICAL PUBLICATION. Reports of completed research or a major significant phase of research that present the results of NASA programs and include extensive data or theoretical analysis. Includes compilations of significant scientific and technical data and information deemed to be of continuing reference value. NASA counter-part of peer-reviewed formal professional papers, but has less stringent limitations on manuscript length and extent of graphic presentations.

- TECHNICAL MEMORANDUM. Scientific and technical findings that are preliminary or of specialized interest, e.g., "quick-release" reports, working papers, and bibliographies that contain minimal annotation. Does not contain extensive analysis.

- CONTRACTOR REPORT. Scientific and technical findings by NASA-sponsored contractors and grantees.

- CONFERENCE PUBLICATION. Collected papers from scientific and technical conferences, symposia, seminars, or other meetings sponsored or co-sponsored by NASA.

- SPECIAL PUBLICATION. Scientific, technical, or historical information from NASA programs, projects, and missions, often concerned with subjects having substantial public interest.

- TECHNICAL TRANSLATION. English-language translations of foreign scientific and technical material pertinent to NASA's mission.

For more information about the NASA STI program, see the following:

- Access the NASA STI program home page at http://www.sti.nasa.gov

- E-mail your question to help@sti.nasa.gov

- Fax your question to the NASA STI Information Desk at 757-864-6500

- Telephone the NASA STI Information Desk at 757-864-9658

- Write to:
  NASA STI Program
  Mail Stop 148
  NASA Langley Research Center
  Hampton, VA 23681-2199

NASA/TM—2019-220184

Vortex Radiometry: Fundamental Concepts

Peter J. Schemmel
Glenn Research Center, Cleveland, Ohio

National Aeronautics and
Space Administration

Glenn Research Center
Cleveland, Ohio 44135

April 2019

Acknowledgments

This work is funded by the NASA Space Communication and Navigation Program, and is protected by a NASA New Technology Report and U.S. Provisional Patent.

Level of Review: This material has been technically reviewed by technical management.

Available from

NASA STI Program
Mail Stop 148
NASA Langley Research Center
Hampton, VA 23681-2199

National Technical Information Service
5285 Port Royal Road
Springfield, VA 22161
703-605-6000

This report is available in electronic form at http://www.sti.nasa.gov/ and http://ntrs.nasa.gov/

Vortex Radiometry: Fundamental Concepts

Peter J. Schemmel
National Aeronautics and Space Administration
Glenn Research Center
Cleveland, Ohio 44135

Abstract: Vortex radiometers (VRs) enable communication systems to maximize data throughput by determining when to employ fade mitigation most efficiently. With this information, communication systems can optimize mitigation strategies before actual fades occur. Doing so maximizes the time over which the link is available, and therefore maximizes data throughput. This paper presents the fundamental concepts of vortex radiometry, including the creation of annular beam patterns through the use of orbital angular momentum (OAM). These concepts are simulated on a 100 Mbps GEO-to-ground Ka-Band communication link. During the simulation a noise source traverses across the link, and without VR capabilities the link is disrupted. However, when the situation is repeated with VR capabilities enabled, the antenna is able to increase receiver gain and maintain the link. VRs are uniquely suited to provide communication systems with the ability to optimize receiver parameters and maximize data throughput, making them critical to enabling next generation communication networks.

1. Introduction

Reliably maximizing data throughput is the goal of every communication system. In the case of NASA for example, increased data throughput means that robotic missions to Mars can incorporate additional science instruments producing more sophisticated data. This enables missions to increase their scientific return and hence be more efficient from a cost perspective.

Data throughput limits also cap how much information space telescopes can transmit back to Earth. This is especially true of observatories such as Kepler, where on-board processing and data reduction were required because the communication system could not handle the enormous amounts of raw data produced [1]. Increasing data throughput reduces on-board processing requirements for space science missions. NASA's continued success in exploration clearly depends on the agency's ability to develop advanced communication systems capable of reliably transmitting more data.

One method to improve data throughput is to increase the data rate, or speed at which information is sent. Data rates have improved steadily over the past few decades. NASA is currently transitioning from X-Band to K/Ka-Band and even optical carrier frequencies in an effort to increase data rates [2–4]. Advanced modulation and coding schemes, as well as multi-beam and multi-polarization systems have achieved additional data rate improvements. Regardless of the data rate however, communication is halted if the link becomes unavailable.

Free space communication links are susceptible to adverse weather, signal interference and jamming. Any of these can reduce, or even halt the flow of data. Occasional disruptions to consumer satellite TV links are acceptable from a safety perspective. However, it is certainly not acceptable to lose communication with astronauts on a spacewalk around the International Space Station, for example. Therefore maximizing data throughput is not only a matter of increasing the data rate, it also requires maximum link availability.

Communication links become unavailable when there is not enough signal at the receiver to overcome the background noise. Fade mitigation techniques [5] are used to overcome these disruptions. Examples include increasing transmitter power, adjusting the carrier frequency, changing the modulation or coding scheme, switching to a different location or simply waiting for a period of time before communicating again. However, excessive use of fade mitigation can lead to increased operational costs as well as reduced RF component lifetimes [6].

The fundamental challenge is to determine how to efficiently and effectively use fade mitigation techniques to maximize data throughput in the presence of adverse weather and signal interference. This is not a novel research topic. NASA, for example, is heavily focused on developing cognitive antennas and networks [7, 8] that autonomously allocate spectrum to multiple users and mitigate interference from unknown sources. There are also several research papers that outline methods to predict signal attenuation levels based on current and historical link statistics [9, 10].

Using the link itself does not provide a significant amount of lead time to select an optimal mitigation strategy, however. Often a single mitigation technique is simply enabled or disabled when a fade is present. Selecting a particular mitigation technique out of a set of available techniques, based on measured link and environmental characteristics would certainly be more effective. The challenge is to identify impending fades, with enough lead time so that the communication system can determine the most effective strategy.

2. Monitoring Link Margins

Communication links fade when their power margins turn negative. The power margin is a measure of the residual signal strength at the receiver, beyond which is required to close the link. Power margins are designed to accommodate small changes in signal strength and ambient noise, ensuring that the link remains available. However, large power margins tend to be avoided, especially in commercial satellite systems, due to increased component weight and thermal management requirements associated with higher power systems [11].

The power margin itself can be defined as,

$$\Delta = 10 \log_{10} \left(\frac{EsNO_{Rcvd}}{EsNO_{Req}} \right), \tag{1}$$

where $EsNO_{Req}$ is the energy per symbol to noise power spectral density required to close the link and is a function of the modulation, coding scheme and desired bit error rate. $EsNO_{Rcvd}$ is,

$$EsNO_{Rcvd} = \left(\frac{RCoNO}{R_{sRF}} \right). \tag{2}$$

Here, R_{sRF} is the symbol rate in (Sym/Sec) and,

$$RCoNO = \left(\frac{P_{Rcvd}}{T_{sys} k_b} \right), \tag{3}$$

with k_b as Boltzmann's constant. The system noise temperature T_{sys} is a summation of all the individual antenna and receiver noise temperatures, including the sky brightness temperature [12]. Power received (P_{Rcvd}) is the product of the transmitter's EIRP, free space and atmospheric path losses and gain of the receiving antenna. Clearly, the link power margin diminishes as the system temperature increases, or the received power decreases.

Fortunately, microwave radiometers are capable of measuring noise powers and hence sky brightness temperatures [13]. Atmospheric effects on radio wave propagation are studied extensively using radiometric data [14, 15]. Rain, clouds, fog and snow are all known to increase sky brightness temperature [11, 16], and contribute to fades on communication links. Radiometers also measure interfering signals, via an increase in noise power, which are interpreted as higher sky brightness temperatures. So, the factors that disrupt communication link availability, and hence reduce data throughput, are identifiable using radiometric measurement techniques.

Interestingly, techniques developed at NASA [17, 18] can collect radiometric data from the communication link itself, and doing so can help warn of impending fades. However, since the communication link itself is being monitored, the lead times are not desirable. Providing ample time to determine 1) if fade mitigation is necessary and 2) what type of mitigation is needed,

requires radiometric data measured around the communication link. Ideally, an annulus or series of concentric rings should be used to measure radiometric data around the link (Fig. 1).

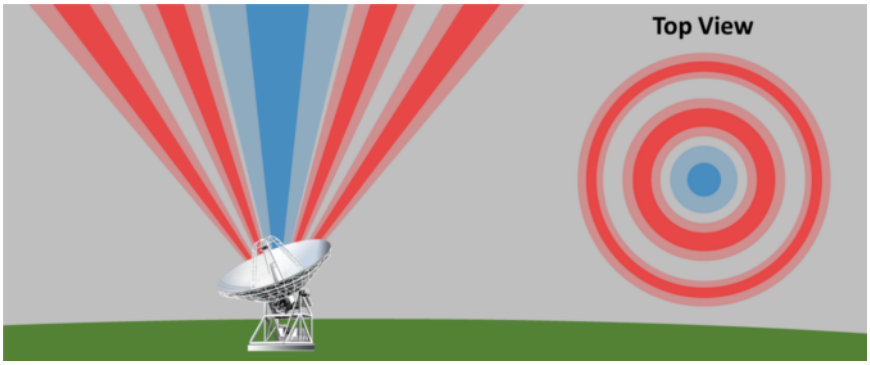

Fig. 1: Concentric annular radiometric beam patterns (red) can be used to determine fade characteristics prior to a noise source impinging upon the communication link (blue).

3. Vortex Radiometry

Creating an antenna capable of measuring radiometric data in annular rings centered on a communication link is a challenge. It is possible to surround a communication antenna with several radiometers, but this is clearly not cost effective. It is also possible to dynamically steer a phased array antenna beam concentrically around the communication link, however this is a high complexity — high cost solution that is impractical for most scenarios. Instead a simple low-cost solution that can be retrofitted to existing antenna systems and integrated into future designs is required. One method is to exploit the orbital angular momentum (OAM) property of light.

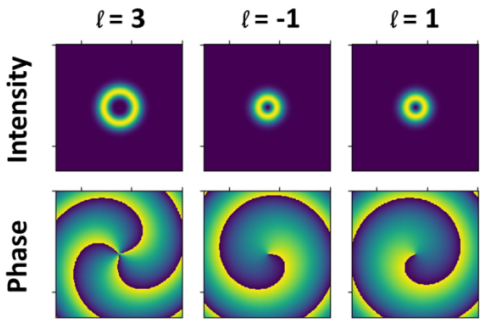

(a) Intensity and phase patterns of OAM beams with various azimuthal mode numbers.

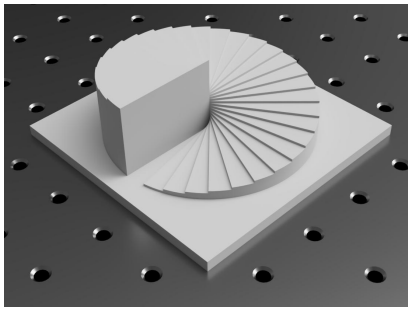

(b) Rendering of a PTFE spiral phase plate, designed to create OAM with an azimuthal mode number of ±1, at 26 GHz.

Fig. 2: The intensity and phase of OAM beams (a) can be manipulated by SPPs (b). Note that the magnitude of the azimuthal mode number defines the number of cuts in the phase pattern, while the sign of the azimuthal mode number defines the sense of rotation.

Within the last decade, several demonstrations have shown that radio waves can possess OAM [19, 20]. Waves carrying OAM exhibit a $2\pi l$ azimuthal phase shift, normal to the propagation axis, where l is the azimuthal mode number [21], ranging from ($-\infty$ to $+\infty$). The magnitude of l defines the number of branch points [22] within the electric field, while the sign

of l defines the rotational direction of the azimuthal phase shift. Viewed in three dimensions, waves carrying OAM contain l number of helically wrapped phased planes. This helical phase structure has led some to colloquially identify these waves as "vortex beams."

While the phase of a wave with OAM is helical, the intensity pattern is annular [23]. This is a result of the phase being undefined at each branch point. The undefined phase means that the electric field is undefined, and without a field it is impossible to have any field intensity. The annular ring's radius of maximum intensity is a function of l such that [24],

$$r_{max} = \omega\sqrt{\frac{|l|}{2}}, \tag{4}$$

where ω is the beam radius [25]. Therefore, increasing the magnitude of l increases the radius of the annular intensity ring Fig. 2a. Imparting OAM of different magnitudes into the electric fields received by the radiometer, then creates concentric beam patterns that can measure radiometric data.

There are numerous methods to impart OAM into an electric field [26, 27], however the simplest method remains the spiral phase plate (SPP) [28]. Spiral phase plates consist of a helically ramped dielectric material Fig. 2b, with a step height h tuned so that the phase thickness is a multiple of $2\pi l$, where λ is the wavelength and n is the refractive index.

$$h = \frac{\lambda \cdot (l_{out} - l_{in})}{n_{spp} - n_{air}} \tag{5}$$

For large changes in azimuthal mode number, the step height h can become unreasonably large. This is alleviated by creating a modular SPP [29], consisting of $|l|$ individual $\Delta l = 1$ SPPs combined together. Imparting OAM into an electric field, using an SPP, is as simple as placing the SPP in front of the antenna aperture [30].

Efficiently applying fade mitigation in order to maximize data throughput requires radiometric data measured from an annular ring around the communication link. This is achievable by imparting OAM, with different azimuthal mode number magnitudes, into the received electric field by using SPPs placed in front of the antenna aperture. "Vortex Radiometers," (VRs) is the suggested name for such systems. The following section numerically demonstrates how VRs are used to enhance communication systems.

4. Simulation

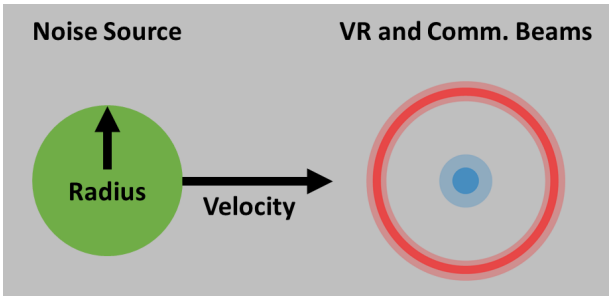

Fig. 3: Numerical simulations record mesaured brightness temperature on a communication link surrounded by a single VR beam, as a function of noise source radius, temperature and velocity.

This section describes a set of numerical simulations that illustrate the impact of using VRs to enhance communication link capabilities. The primary objectives are to 1) show that VRs can be used to maintain a link in the presence of a noise source capable of producing a fade and 2) that

the lead time measured by the VR is greater than if the communication link itself was used to measure the radiometric data. In this particular scenario the communication antenna increases RF receiver gain to mitigate the fade.

Simulated Communication Link Parameters

Parameter	Value	Units
Frequency	26	GHz
Transmitter Power	0.75	W
Transmitter Aperture Diameter	0.55	m
Modulation	BPSK	-
Coding Scheme	Uncoded	-
Data Rate	100	Mbps
BER	1E-6	-
Range	35786	km
Receiver Aperture Diameter	1.2	m
Sky Brightness Temperature	40	K
Sky Brightness Temperature Standard Deviation	0.25	K
VR OAM Beam Az. Mode Number	20	-
Additional Fade Mitigation Receiver Gain	60	dB
Noise Temperature Threshold	42	K

Table 1

To accomplish this, a simulated communication link is established between a ground station antenna and GEO stationary satellite. Parameters of the link are shown in Table 1. A noise source with parameters detailed in Table 2 traverses across the communication link (Fig. 3) at an altitude of 6,000 meters while the communication link margin is monitored as a function of time.

Noise Source Parameters

Parameter	Value	Units
Brightness Temperature	20	K
Attenuation and Scattering Factor	0.015	dB/K
Radius	50 , 100 , 500	m
Altitude	6000	m
Velocity	10	m/s

Table 2

The simplest VR based fade mitigation algorithm relies solely on measured sky brightness

temperatures from the VR and communication link. When brightness temperature, measured by the VR, is above some threshold fade mitigation is enabled. Mitigation is disabled when the VR measured brightness temperature falls below the threshold AND the noise temperature measured on the communication link is less than that measured by the VR. Automatic determination of the threshold temperature is the subject for another paper. Here, it is sufficient to use a static threshold that is well above the clear sky brightness temperature, including its statistical variations. This simulation uses a threshold value of 42 K. For simplicity, this paper assumes that the communication link will attenuate by 0.015 dB / K of brightness temperature. Such a simple correlation is not realized in actuality (consider the case of scattering by heavy rain fall), but it serves as a good first approximation. Practical VR systems will require sophisticated RF-weather models in order to accurately assess the proper level of correlation. This is an important avenue for future research.

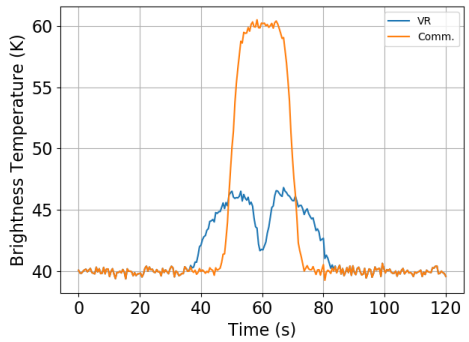

(a) Measured brightness temperature for a noise source with a 100 m radius

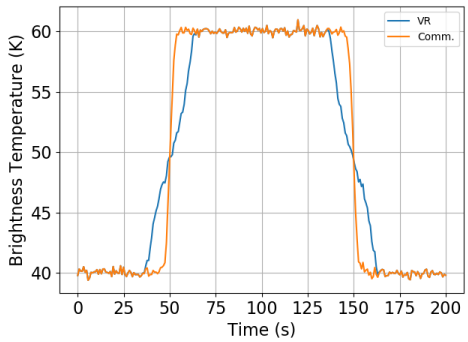

(b) Measured brightness temperature for a noise source with a 500 m radius

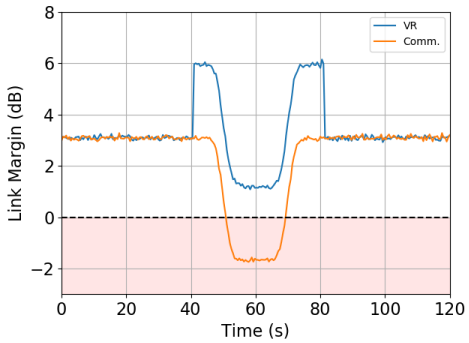

(c) Link margin for a noise source with a 100 m radius

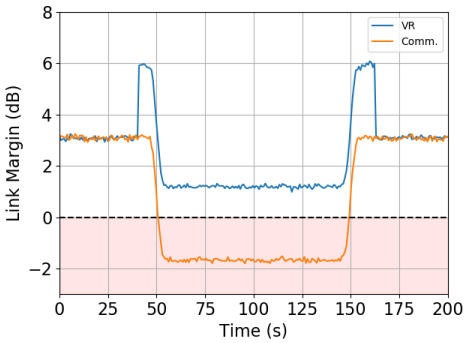

(d) Link margin for a noise source with a 500 m radius

Fig. 4: Sky brightness temperature and link power margin measured by VR and communication link, for two different noise source parameters. The VR successfully enables fade mitigation to maintain the link.

Examining Fig. 4 clearly shows that VRs are capable of enabling fade mitigation techniques to maintain a link during a fade event. As one may suspect, the effectiveness of the VR system is a function of noise source parameters and the maximum intensity radius of the annular beam pattern. For example, a noise source with a small radius can cause the VR to disable fade mitigation prematurely. Reducing the azimuthal mode number of the VR beam decreases the beam's radius and remedies the situation (Fig. 5).

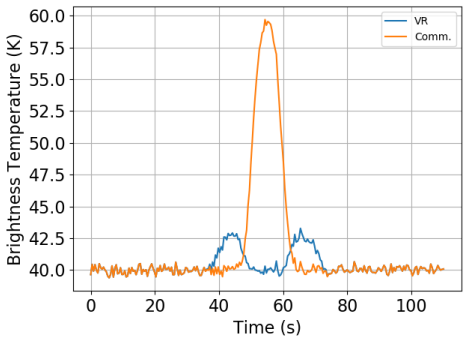

(a) Brightness temperature measured using an azimuthal mode number of 20 and a noise source with a 50 m radius.

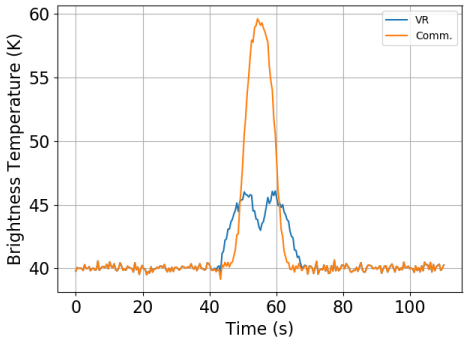

(b) Brightness temperature measured using an azimuthal mode number of 5 and a noise source with a 50 m radius.

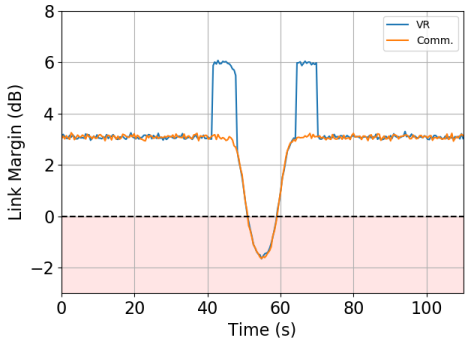

(c) Link margin measured using an azimuthal mode number of 20 and a noise source with a 50 m radius.

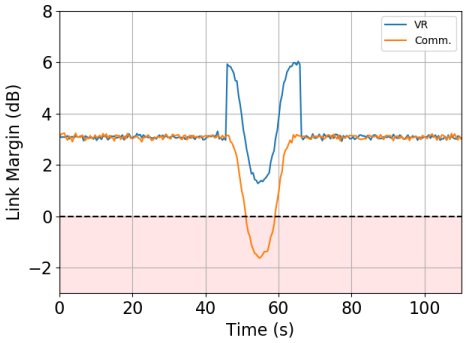

(d) Link margin measured using an azimuthal mode number of 5 and a noise source with a 50 m radius.

Fig. 5: A noise source with a radius of 50 m traverses the communication link. Reducing the azimuthal mode number from 20 to 5 ensures that the fade is mitigated properly. This is evidence to suggest that future VR systems will require multi-beam capabilities.

Small noise source mitigation is achieved by reducing the VR beam's radius. However, it is also evident that changing the VR beam's radius also changes the lead time between engaging mitigation and the actual fade event. Exploring this further addresses the second objective, which is to show that VRs produce longer lead times compared to using the communication link itself.

Running successive simulations while increasing the VR beam's azimuthal mode number produces Fig. 6. Lead times are defined to be the time between initiating fade mitigation and the time at which the link would first experience a fade. The Y-axis shows the percent increase in lead time, which is normalized to the lead time calculated using the communication link itself. The results show that regardless of noise source size, VRs produce significantly longer lead times. This is critically important to the development of next generation communication systems, which will need additional time to optimize fade mitigation strategies.

5. Conclusion

Future space exploration missions will place significant pressure on their communication systems, requiring ever increasing data throughput capabilities. This demand must be met with

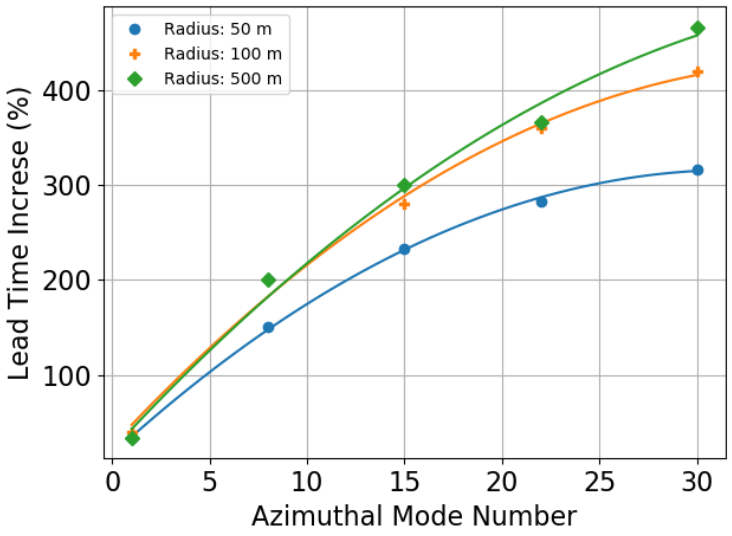

Fig. 6: Using VRs to determine if a noise source is approaching, results in a significant increase in fade detection lead times. The effect becomes more pronounced as the VR's azimuthal mode number is increased.

improvements to both achievable data rates and link availability. A suite of fade mitigation techniques will be available to next generation communication systems, which will need to optimize mitigation strategies in order to maximize data throughput.

Vortex Radiometers (VRs) achieve this goal by using annular beam patterns to detect noise sources well before they interact with the communication link. Using SPPs to impart OAM into the antenna beam generates annular beam patterns capable of measuring radiometric data. Changing SPP geometry adjusts the size of the annular beam, which was shown to be useful in detecting noise sources of various sizes. Increasing the annular radius significantly impacts the lead time as well. A series of numerical simulations showed that VRs are superior to using the communication link itself, in determining when to enable fade mitigation.

This paper's aim was to present the fundamental concepts of vortex radiometry. Despite using a simplistic algorithm, the numerical simulations presented herein demonstrate that VRs provide a substantial impact to communication system capabilities. A second paper in this series will outline a more advanced algorithm, utilizing multiple VR beams, to determine 1) when a fade will occur, 2) how long the fade will persist for and 3) how intense the fade will be. Future work will demonstrate how the increased lead times generated by VRs will enable cognitive antennas to determine an optimal fade mitigation technique from a suite of possible solutions.

Finally, a two-mode VR is in use at NASA's Glenn Research Center in Cleveland, Ohio. It is currently undergoing testing to validate the concepts presented in this paper. Results from this testing, along with details of the VR design and construction will be presented in a future report. Upon validation, the VR will monitor a static GEO satellite link, with the aim of increasing link availability. The ultimate objective is to integrate VR technology into NASA's space communication networks.

References

1. D. G. Koch, W. Borucki, E. Dunham, J. Geary, R. Gilliland, J. Jenkins, D. Latham, E. Bachtell, D. Berry, W. Deininger, R. Duren, T. N. Gautier, L. Gillis, D. Mayer, C. D. Miller, D. Shafer, C. K. Sobeck, C. Stewart, and M. Weiss, "Overview and status of the Kepler Mission," in *Optical, Infrared, and Millimeter Space Telescopes,* vol. 5487 (2004), pp. 1491–1500.
2. D. M. Cornwell, "NASA's optical communications program for 2015 and beyond," in *Proc. SPIE,* vol. 9354 (2015), pp. 9354 – 9356.
3. D. M. Cornwell, "NASA's optical communications program for 2017 and beyond," in *2017 IEEE International Conference on Space Optical Systems and Applications (ICSOS),* (2017), pp. 10–14.
4. R. LaBelle and D. Rochblatt, "Ka-band high-rate telemetry system upgrade for the NASA deep space network," Acta Astronaut. **70**, 58 – 68 (2012).
5. A. D. Panagopoulos, P. M. Arapoglou, and P. G. Cottis, "Satellite communications at KU, KA, and V bands: Propagation impairments and mitigation techniques," IEEE Commun. Surv. Tutorials **6**, 2–14 (2004).
6. D. J. Cheney, E. A. Douglas, L. Liu, C. F. Lo, B. P. Gila, F. Ren, and S. J. Pearton, "Degradation mechanisms for GaN and GaAs high speed transistors," Materials **5**, 2498–2520 (2012).
7. W. D. Ivancic, P. E. Paulsen, K. R. Vanden, and D. S. Ponchak, "Cognitive networking with regards to NASA's Space Communication and Navigation Program," NASA Tech. Memo. 2013-216585 (2013).
8. R. Roche, J. C. Briones, and B. N. Kowaleski, "Metabrain for embedded cognitition (MBEC)," NASA Tech. Memo. 2018-219877 (2018).
9. M. M. J. L. van de Kamp, "Short-term prediction of rain attenuation using two samples," Electron. Lett. **38**, 1476–1477 (2002).
10. B. Gremont, M. Filip, P. Gallois, and S. Bate, "Comparative analysis and performance of two predictive fade detection schemes for Ka-band fade countermeasures," IEEE J. on Sel. Areas Commun. **17**, 180–192 (1999).
11. B. R. Elbert, *Introduction to Satellite Communication* (Boston, Massachusetts: Artech House, 1987).
12. T. L. Wilson, K. Rohlfs, and S. Huttemeister, *Tools of Radio Astronomy* (Berlin: Springer, 2009).
13. T. Y. Otoshi, *Noise Temperature Theory and Applications for Deep Space Communication Antenna Systems* (Boston, Massachusetts: Artech House, 2008).
14. J. Nessel, M. Zemba, and J. Morse, "Results from three years of Ka-band propagation characterization at Svalbard, Norway," in *2015 9th European Conference on Antennas and Propagation (EuCAP),* (2015), pp. 1–5.
15. M. Zemba, J. Nessel, J. Houts, N. Tarasenko, S. Lane, and D. Murrell, "Preliminary results from the AFRL-NASA W/V-band terrestrial link experiment in Albuquerque, NM," in *2016 IEEE International Symposium on Antennas and Propagation (APSURSI),* (2016), pp. 1249–1250.
16. M. A. Janssen, *Atmospheric Remote Sensing By Microwave Radiometry* (New York: John Wiley, 1993).
17. M. Zemba, J. Nessel, L. Luini, and C. Riva, "Comparison of integrated digital radiometer with concurrent water vapor radiometer using the alphasat receivers in Milan, Italy," in *13th European Conference on Antennas and Propagation (EuCAP),* (2019).
18. J. Nessel, G. Goussetis, M. Zemba, and J. Houts, "Design and preliminary results from Ediburgh, UK Alphasat Q-Band Propagation Terminal," in *22nd Ka and Broadband Communications Conference,* (2016).
19. M. D. Gray, G. Pisano, S. Maccalli, and P. Schemmel, "Amplification of OAM radiation by astrophysical masers," Mon. Notices Royal Astron. Soc. **445**, 4477–4503 (2014).
20. L. Allen, M. W. Beijersbergen, R. J. C. Spreeuw, and J. P. Woerdman, "Orbital angular momentum of light and the transformation of Laguerre-Gaussian laser modes," Phys. Rev. A **45**, 8185–8189 (1992).
21. G. Turnbull, D. Robertson, G. Smith, L. Allen, and M. Padgett, "The generation of free-space Laguerre-Gaussian modes at millimetre-wave frequencies by use of a spiral phaseplate," Opt. Commun. **127**, 183 – 188 (1996).
22. D. J. Sanchez and D. W. Oesch, "The aggregate behavior of branch points: the creation and evolution of branch points," in *Proc. SPIE,* vol. 7466 (2009), pp. 7466 – 7478.
23. J. Leach, M. J. Padgett, S. M. Barnett, S. Franke-Arnold, and J. Courtial, "Measuring the orbital angular momentum of a single photon," Phys. Rev. Lett. **88**, 257901 (2002).
24. M. J. Padgett, F. M. Miatto, M. P. J. Lavery, A. Zeilinger, and R. W. Boyd, "Divergence of an orbital-angular-momentum-carrying beam upon propagation," New J. Phys. **17**, 023011 (2015).
25. P. F. Goldsmith, *Quasioptical Systems : Gaussian Beam Quasioptical Propagation and Applications* (New Jersey : IEEE Press, 1998).
26. M. Mirhosseini, O. S. Magaña-Loaiza, C. Chen, B. Rodenburg, M. Malik, and R. W. Boyd, "Rapid generation of light beams carrying orbital angular momentum," Opt. Express **21**, 30196–30203 (2013).
27. S. Maccalli, G. Pisano, S. Colafrancesco, B. Maffei, M. W. R. Ng, and M. Gray, "Q-plate for millimeter-wave orbital angular momentum manipulation," Appl. Opt. **52**, 635–639 (2013).
28. P. Schemmel, S. Maccalli, G. Pisano, B. Maffei, and M. W. R. Ng, "Three-dimensional measurements of a millimeter wave orbital angular momentum vortex," Opt. Lett. **39**, 626–629 (2014).
29. P. Schemmel, G. Pisano, and B. Maffei, "Modular spiral phase plate design for orbital angular momentum generation at millimetre wavelengths," Opt. Express **22**, 14712–14726 (2014).
30. E. Doumanis, D. Zelenchuk, V. Fusco, and G. Goussetis, "Conical horn antenna with spiral phase plate for difference pattern generation," in *2013 7th European Conference on Antennas and Propagation (EuCAP),* (2013), pp. 1309–1312.